NMR Study of Antiferromagnetic Mn alloys

Hisashi Takenaka

March 1973

ABSTRACT

The NMR signals of Mn^{55} in various antiferromagnetic Mn alloys have been observed in liquid helium temperature range. The internal field of Mn^{55} in antiferromagnetic b.c.c. Cr-Mn alloys decreases with the concentration of Mn from 62.3 kOe to 39.0 kOe. It seems that the magnetic moment of Mn decrease. The nuclear spin-lattice relaxation of Mn^{55} in antiferromagnetic Cr-Mn alloys is explained by the same mechanism as that in paramagnetic b.c.c. transition alloys, Ti-V, V-Cr, and V-Mn. The internal field of Mn^{55} in antiferromagnetic γ Mn (f.c.c. or f.c.t.) is 65.2 kOe, and this is very small from the consideration of the value of the magnetic moment of 2.4 μ_B . The satellite signals appear at the field of about 95 kOe which is almost independent of the species of the impurity atoms in the dilute alloys. The small internal field indicates that a large positive contribution is needed to compensate a large negative core polarization term. The appearance of one satellite at a considerably higher frequency than the main line indicates that the compensation is the property of the Mn atom itself and the effect of the impurity atom is well limited to its nearest neighbors. This concept is useful also to explain the internal fields in the γ Mn alloys of high concentration range.

CONTENTS

§ 1. Introduction.

Manganese metal and alloys have a variety of magnetic properties. They have been current interest for many physicists. It is interesting to do the experiment of NMR for understanding the electronic structure of such materials.

Body centered cubic chromium-manganese alloys are obtainable in the concentration range between pure Cr and about 70 at.% of Mn. These alloys are antiferromagnetic except for dilute Mn alloys, which are magnetically ordered in sinusoidal spin density wave state.[1-3] Néel temperature of the alloys increases with Mn concentration from 310 K for pure Cr metal to 790 K for 50 at.% Mn alloy.[2),4)] The magnetic structure of antiferromagnetic Cr-Mn alloy is shown in figure 1. The average magnetic moments of the alloys, obtained by neutron diffraction experiments,[1),2)] are almost constant over whole concentration range of b.c.c. alloy except for the dilute Mn alloys. The dilute alloys and pure Cr metal are well described by itinerant electron model.[1),3)] The validity of this model has not been confirmed as the Mn concentration becomes large.[5)]

NMR experiments have been performed in paramagnetic b.c.c. Ti-V, V-Cr, and V-Mn alloys.[6),7),8)] The electron number dependence of the nuclear spin-lattice relaxation times of V^{51} and Mn^{55} in these alloys is well explained by the change of the density of states at the Fermi level determined by the coefficient of the electronic specific heat. It is interesting to investigate this relation in antiferromagnetic b.c.c. Cr-Mn alloys.

On the other hand, γ Mn metal and alloys, which are antiferromagnetic, have face centered cubic or face centered

tetragonal structures.[9-13] Néel temperature of γ Mn metal is about 500 K. According to the neutron diffraction experiments, the magnetic moments have the magnitude, 2.4 μ_B. The magnetic structure is also shown in figure 1. The f.c.c. γ Mn becomes f.c.t. below the Néel temperature. Because pure γ Mn is not stable at low temperatures, small amounts of impurity, such as Cu, Au, Pd, Ir, Ni, etc., are added generally to stabilize the γ phase. This addition causes small ambiguity in the physical quantities but does not change the fundamental properties of γ Mn. As the impurity concentration becomes large, the tetragonal distortion does not occur. The γ Mn is theoretically explained by the gapless band antiferromagnetism,[14] which is usefull to understand its properties qualitatively. The magnetic structures of γ Mn alloys show complicated behavior with alloying composition.

In the present work, NMR of Mn^{55} in antiferromagnetic Cr-Mn and γ Mn alloys were observed in order to study the electronic state in these alloys.

§ 2. Experimental procedures.

A) Sample preparations.

1) Cr-Mn alloys.

The Cr-Mn samples were prepared by argon arc melting with turning and remelting the buttons of alloys repeatedly for homogenization. Purities of Cr and Mn metals are 99.999 % and 99.99 % respectively. The ingots were crushed into grains and then powdered by an agate mortar. The sample size is smaller than 70 μ. The concentrations of the alloys were determined by chemical analysis and the b.c.c. structures of the powdered samples were confirmed by X-ray diffraction. Especially, two samples were prepared for 28.9 at.% Mn alloys to investigate the homogeneity of the alloy ; one was powdered without any heat treatment after an arc melting and the other was powdered after heat treatment of keeping the ingot at 1600°C for 30 hours. NMR signals of those two samples have no difference, so that all samples are expected to be well homogenized even without such heat treatment.

2) γ Mn alloys.

The γ phase samples of Mn alloys were made with the addition of Cu, Ni, Pd, Au, Ir, or Fe metals which are all more than 99.9 % pure. The mixtures of metals were melted by induction melting in corundum crucibles in an argon atmosphere. The ingot was sealed in a quartz tube filled with pure argon gas at a pressure of 150 mmHg and kept at the temperature of just below the upper limit of γ phase region for 20 hours. A sharp quenching was obtained by breaking the tube in ice water. After these heat treatments, the ingots were filed and powdered by an agate mortar. The sample size is smaller than 70 μ. As the γ-phase of the Mn-Fe alloys of

composition less than 40 at.% Fe is not stable at low temperature, 5 at.% Cu impurity was added to stabilize the γ phase. This addition of Cu impurity does not change much the physical properties of γ Mn-Fe alloy.[13] The f.c.t. or f.c.c. structures of the powdered samples were confirmed by X-ray diffraction. All the samples except for 2.5 at.% Ni alloy had a single γ phase. The 2.5 at.% Ni alloy was composed of the two phases of γ and β. The admixture of β phase has no effect on NMR experiment in γ Mn because the NMR frequency of β Mn is zero in zero external field. This point will be discussed in later section.

B) NMR technique.

The NMR experiment was carried out with frequency variable spin echo technique under zero external field. A block diagram showing the essential features of our NMR system is shown in figure 2. Additional supplementary equipments are needed for frequency determination, power measurements, gain calibration, etc. The frequency was varied with intervals of 2 MHz from 18 MHz to 100 MHz for Cr-Mn alloys and to 250 MHz for γ Mn alloys. For some typical samples, the frequency was swept up to 350 MHz to confirm the absence of signals at higher frequencies. H_1 (rf field strength) used in this experiment was about 60 Oe, which was kept as constant as possible over the above frequency range. To obtain an information below 18 MHz, NMR was observed using an apparatus with the fixed frequency of 10 MHz by applying an external field. Spin echo signal was obtained by the first 90° and second 180° pulses. The nuclear spin-lattice relaxation time, T_1, was measured by observing spin echo signals after a comb of saturation pulses. It was confirmed that the saturation was sufficiently achieved by the

comb. Gain of receiving system after the saturating pulse train and two spin echo pulses was monitored by observing the out-put of a test signal applied to the sample coil by electromagnetic coupling. The internal field measurement was performed at 1.4 K and T_1 measurement was done at 1.4 K and 4.2 K. The temperature was determined by the vapor pressure of liquid helium. The magnetic moment is expected to be sufficiently saturated at liquid helium temperatures. For the line shape determination, the echo amplitude extrapolated to $\tau=0$ (τ the separation of two pulses) is used in order to avoid the effect of transverse relaxation time. The gain difference of the receiver system caused by the change of the frequency was also calibrated by the test signal. To obtain the true line shape, we must consider this gain difference and other factors such as the difference in Boltzmann factor. In order to eliminate these ambiguities, we used the signals of Mn^{55} in antiferromagnetic α Mn metal at site 1 (199.4 MHz), site 2 (151.5 and 144.5 MHz), and site 3 (31.0 and 26.5 MHz), of which the ratios of the numbers of atoms are 1:2:2:4:8.[15] We obtained the line shapes using such correction that the intensity ratio of these α Mn signals becomes 1:2:2:4:8. The internal field was evaluated, using the nuclear g-value obtained by the resonance frequency of Mn^{55} of 10.500 MHz at 10 kOe.[16]

§ 3. Experimental results.

A) Cr-Mn alloys.

Figure 3 shows the line shape of Mn^{55} in the 28.9 at.% Mn alloy obtained at 1.4 k. All the Cr-Mn samples of different concentrations have the similar line shapes to that in figure 3. The internal field is calculated from the peak frequency of the line. Figure 4 shows the concentration dependence of the internal field of Mn^{55} in the antiferromagnetic Cr-Mn alloys at 1.4 k. The same results are obtained at 4.2 K. The intensity of NMR signals is proportional to the Mn concentration. The values of magnetic moments of Mn and Cr are expected to be almost the same in sinusoidal spin density wave phase, and it seems probable that the moments of Mn do not change much even in antiferromagnetic alloys as far as the concentration of Mn is sufficiently dilute. Therefore, it is expected that the Mn moment is almost the same as the average moment in these alloys.
The internal field of Mn^{55} is estimated to be 85 kOe per Bohr magneton in the 3.0 at.% Mn alloy using the value of average moment of 0.73 μ_B measured by neutron diffraction experiment.[1),2)] This is in agreement with the value of about 75 kOe per Bohr magneton in antiferromagnetic α Mn metal[15)]. Figure 5 shows the concentration dependence of the full half-value width of the lines. The product of the nuclear spin-lattice relaxation time, T_1, and the temperature, T, is shown in figure 6. Here T_1 was measured at 1.4 K and 4.2 K. In the 4.7 at.% Mn alloy, T_1 was measured only at 1.4 K because of the poor intensity at 4.2 K. The value of T_1T is constant in the temperature region from 4.2 K to 1.4 K. It varies drastically with the Mn concentration.

B) γ Mn alloys.

The line shapes of the Mn^{55} in the γ Mn alloys with various impurities are shown in figure 7. They are similar for all the alloys of the same concentration. There are two peaks. The main peak appears at about 70 MHz and the satellite at about 100 MHz. The intensity of main peak decreases with the impurity concentration and that of satellite increases. The ratio of these intensities is listed in table. If the main peak and satellite are attributed to the nuclei that have zero impurity atom and one impurity atom in their nearest neighbors respectively, the intensity ratio of these signals is expressed as

$$\left(I_{sat} / I_{main} \right)_{cal} = 12c(1-c)^{11}/(1-c)^{12}=12c/(1-c),$$

where c is the concentration of impurity. The experimental values well agree with the calculated ones. Therefore, the impurity seems to have a perturbing effect only on its nearest neighbors in γ Mn metal. The main signal is considered to be almost the same with the NMR signal in pure γ Mn metal. Thus the internal field of Mn^{55} is estimated to be 65.2 kOe, which is in agreement with the value of 65 kOe obtained by nuclear specific heat measurement.[17] Using the value of magnetic moment, 2.4 μ_B, measured by neutron diffraction experiment,[10] the internal field of Mn^{55} is calculated to be 27.2 kOe per Bohr magneton. This value is too small in comparison with 75 kOe or 85 kOe per Bohr magneton in antiferromagnetic α Mn metal or Cr-Mn alloys.[15] The line shapes in the higher impurity concentration range and those in the alloys containing other impurities are shown in figure 8, 9, and 10. These line shapes give widely distributed internal fields. The NMR of Cu^{63} and Cu^{65} are also shown in the figure 10. The signals of Cu^{63} and

Cu^{65} can not be distinguished because their resonance frequencies are close to each other and the line shapes are broad in these alloys. The center of gravity of the asymmetric broad line of Mn^{55} is shown in figure 11 in order to make it clear that the dependence of the internal fields on the concentration for various kinds of alloys. Figure 12 shows the integrated intensities of γ Mn alloys, where the broken line indicates the expected intensity. The agreement between the measured and expected intensities indicates that the whole resonance was observed in our measurement in spite of very broad nature of the resonance lines. Only the intensity of 2.5 at.% Ni alloy is about the half of the expected value. This is consistent with the result of the X-ray diffraction investigation, that a considerable amount of β phase exists in the sample as already pointed out in the section 2. The transverse relaxation time, T_2, of Mn^{55} in Mn-Cu alloys is shown in figure 13. T_2 is larger as the concentration of Mn increases. This concentration dependence is contrary to a simple expectation of the increase of the spin-spin coupling by the concentration which holds well in usual alloys.

§ 4. Discussions.

A) Cr-Mn alloys.

1) Internal fields and line widths.

As is seen in figure 4, the internal field of Mn^{55} decreases with the increase of the concentration of Mn in the range from 3 to 40 at.%, and then is almost constant in the range of 40~60 at.%. It seems to indicate that the magnetic moment of Mn decreases with the Mn concentration in the former range. On the other hand, Mössbauer effect measurement of W^{182} doped in the Cr-Mn alloys has been carried out by Kunitomi and Kanashiro.[19] Their result indicates that the internal field of W^{182} increases with the increasing Mn concentration. As W is considered to take place of Cr, the result suggests that the moment of Cr increases with Mn concentration. The average magnetic moment of the Cr-Mn alloys, obtained by neutron diffraction experiment,[2] does not change in the range of 7~50 at.%. These circumstances are shown in figure 14. Thus these results seem to be qualitatively consistent with each other.

The line width increases with the increase of Mn concentration below 40 at.% and is constant in the range of 40~60 at.% Mn. The line width is caused by the distribution of the internal field and this means that the magnetic moments of the Mn also distribute. Some additional broadening will be produced by the electric quadrupole interactions. These distributions of the magnetic moments and the electric field-gradients arise from the statistical distribution of Cr and Mn atoms.

2) Nuclear spin-lattice relaxation times.

The nuclear spin-lattice relaxation in metal is caused by the hyperfine interaction between the nuclear spin and conduction

electrons. According to Korringa,[20] Obata,[21] and Yafet-Jaccarino,[22] T_1 in paramagnetic transition metals or alloys is expressed as follows;

$$1/T_1 = 1/\tau_s + 1/\tau_{cp} + 1/\tau_{orb},$$

$$1/\tau_s = 4\pi k \gamma_n^2 [H_{hf}(s)]^2 \rho_s^2 kT,$$

$$1/\tau_{cp} = 4\pi k \gamma_n^2 [H_{hf}(core)]^2 \rho_d^2 kT \left[\frac{1}{3} f^2 + \frac{1}{2}(1-f)^2\right],$$

$$1/\tau_{orb} = 4\pi k \gamma_n^2 [H_{hf}(orb)]^2 \rho_d^2 kT \left[\frac{2}{3} f\left(2 - \frac{5}{3} f\right)\right],$$

where $1/\tau_s$, $1/\tau_{cp}$, and $1/\tau_{orb}$ are the relaxation rate due to the 4s Fermi contact, 3d core polarization, and the 3d orbital interactions, and $H_{hf}(S)$, $H_{hf}(core)$, and $H_{hf}(orb)$ are the hyperfine fields in the metals or alloys due to these interactions, respectively. The parameter f is the relative weight of Γ_5 and Γ_3 orbitals at the Fermi level. Here the dipolar and electric quadrupole terms are neglected because of their small effects as usual. The ρ_s and the ρ_d are the density of state per atom (for one direction of the spin) of the 4s and 3d bands at the Fermi level.

In usual transition metals and alloys, the contribution of 4s electrons to the relaxation is not important and moreover can be considered nearly independent of the concentration of the alloys. Therefore, the variation of the T_1 is attributed mostly to the change of ρ_d. The coefficient of electronic specific

heat, γ, is proportional to the density of state at the Fermi level. Therefore, a close correlation is expected between T_1 and γ. The electron number dependence of the $(T_1T)^{-1/2}$ of V^{51} in the paramagnetic Ti-V, V-Cr, and V-Mn alloys qualitatively fits to that of γ, measured by Cheng et al.[23], and moreover, if proper values are taken for the above parameters, T_1T can be even quantitatively explained.[6),7),8)] The values of T_1T of Mn^{55} in the paramagnetic V-Mn alloys is also explained by these considerations.

It is interesting that whether or not the value of T_1T in antiferromagnetic Cr-Mn alloys is also explained by the above theory of the itinerant nature of 3d electrons. In this case, however, the values of the density of states of the majority and minority spin bands are needed separately.[24)] Thus, T_1 in antiferromagnetic Cr-Mn alloys is expressed as follows;

$$1/T_1 = 1/\tau_s + 1/\tau_{cp} + 1/\tau_{orb},$$

$$1/\tau_s = 4\pi\hbar\gamma_n^2 [H_{hf}(s)]^2 \rho_{s\uparrow}\rho_{s\downarrow} kT,$$

$$1/\tau_{cp} = 4\pi\hbar\gamma_n^2 [H_{hf}(core)]^2 \rho_{d\uparrow}\rho_{d\downarrow} kT \left[\frac{1}{3}f^2 + \frac{1}{2}(1-f)^2\right],$$

$$1/\tau_{orb} = 4\pi\hbar\gamma_n^2 [H_{hf}(orb)]^2 \frac{1}{2}(\rho_{d\uparrow}^2 + \rho_{d\downarrow}^2) kT \left[\frac{2}{3}f\left(2-\frac{5}{3}f\right)\right],$$

where the arrow expresses the direction of the spins. The density of states obtained from γ is the sum of $\rho_{d\uparrow}$ and $\rho_{d\downarrow}$, as $\rho_{s\uparrow}$ and $\rho_{s\downarrow}$ can be neglected as compared with $\rho_{d\uparrow}$ and $\rho_{d\downarrow}$. Here it is assumed for simplicity that the $(T_1T)^{-1/2}$ is proportional to the γ, which is the average value of the density of states for

majority and minority spin states at the Fermi level. The values of $(T_1T)^{-1/2}$ of V^{51} and Mn^{55} through the b.c.c. alloy-systems from Ti to Mn are shown in figure 15, where △, ×, ●, and ○ show the values of the $(T_1T)^{-1/2}$ of V^{51} in the paramagnetic Ti-V and V-Cr alloys, V^{51} in the paramagnetic V-Mn alloys, Mn^{55} in the paramagnetic V-Mn alloys, and Mn^{55} in the antiferromagnetic Cr-Mn alloys, respectively.[6),7),8)] The γ for Ti-V, V-Cr, and Cr-Mn, obtained by Cheng et al.,[23)] is also shown in figure 15 by the solid line, which is normalized to fit the value of $(T_1T)^{-1/2}$ of Mn^{55} in Cr-Mn alloys at the pure Cr position. As seen in the figure, the $(T_1T)^{-1/2}$ of Mn^{55} in antiferromagnetic Cr-Mn are almost proportional to the γ. The difference of T_1T between V^{51} and Mn^{55} in V-Mn alloys comes mainly from the difference in the hyperfine fields, if we assume the density of states to be common to both atoms. The ratio of $(T_1T)^{-1/2}$ of Mn^{55} and V^{51} amounts to 1.9 . On the other hand, the ratio,

$$(T_1T)^{-1/2} \text{ of } Mn^{55} \text{ in Cr-Mn} \;/\; (T_1T)^{-1/2} \text{ of } V^{51} \text{ in V-Cr} \;,$$

is estimated to be 2.2 when the values of $(T_1T)^{-1/2}$ of both alloys are extrapolated to the pure Cr position. This value of 2.2 agrees well with the ratio, 1.9, obtained for V-Mn alloys. Therefore, spin-lattice relaxation times are smoothly connected across the paramagnetic and antiferromagnetic alloys. This result indicates that the spin-lattice relaxation mechanism is also explained by the same conception in antiferromagnetic Cr-Mn alloys as in paramagnetic transition alloys of Ti-V, V-Cr, and V-Mn. The $(T_1T)^{-1/2}$ of the V^{51} is translated into that of the Mn^{55} by multipling the factor, 2.2, for the Ti-V and V-Cr alloys, which is shown in the figure 15 by the broken line.

B) γ Mn metal.

The numerical value of the internal field of 3d transition elements is theoretically and experimentally given as ∼-100 kOe per Bohr magneton, the main contribution arising from the core polarization.[18] The values, 75 kOe/μ_B in antiferromagnetic α Mn[15] and 85 kOe/μ_B in antiferromagnetic Cr-Mn alloy, are close to the above value, but the value of 27.2 kOe/μ_B in antiferromagnetic γ Mn metal is too small. Therefore, a positive contribution is needed to compensate the core polarization term in γ Mn metal. If the positive contribution arises from the effective field due to the magnetic interaction from the nearest neighbors, satellite lines should appear by the partial breaking of the compensation when a non magnetic impurity is introduced to the site. Furthermore the satellite must be composed of two lines with the intensity ratio of 1:2 at both sides of main peak as the nearest neighbors are constructed of 4 parallel spins and 8 anti-parallel spins. However only one satellite line is observed. This fact suggests that the large positive contribution is the special property of Mn atom itself in γ Mn metal and the origin of the satellite is considered not to be due to the magnetic interaction from the neighbors such as the core polarization or conduction electron polarization by the neighboring moments, but the change of the electronic state on the Mn atom by the existence of the impurity. Several origins can be considered for the positive contribution. For example, the s-d mixing, that is the admixture of 4s electrons into 3d band, will give a positive contribution to the internal field. The large splitting of the satellite from the main line may be the consequence of the decrease of the s-d mixing caused by the nearest neighbor

impurity atom. The s-d mixing is considered to decrease as the Mn atoms are isolated. As mentioned before, the aspect of satellites is independent of the kind of the impurity atoms. This fact shows that the degree of the decrease of the s-d mixing is almost the same in the low impurity concentration range even if the kind of the impurity atoms differs.

C) γ Mn alloys.

Figure 16 shows the average magnetic moments of the γ phase Mn alloys with several impurities obtained by neutron diffraction experiments.[9-13] The simple dilution line in the figure shows the change of the average magnetic moment when the Mn atom has constant magnetic moment and the impurity atom is non-magnetic. The alloys are classified into four types. In the 1st group, the average moment changes along the simple dilution line. The magnitude of the moment on Mn seems to be constant and that on impurity to be zero. Mn-Ni and Mn-Ir alloys belong to this group. In 2nd group, the moment of Mn seems to increase. Mn-Pd alloys belong to this group. If the increase of the average moment is attributed to the magnetic moment of Pd atom, each Pd atom must have 5.5 μ_B. This value is unreasonably large, so that the increase of the moment of Mn atom is plausible. In the 3rd group, the moment of Mn decreases. Mn-Cu alloys belong to this group. Mn-Au alloys also belong to this group. Mn-Fe alloys belong to the 1st group when the concentration of Fe is not large. However as the Mn-Fe alloys are magnetically complicated in the high concentration range of Fe according to the result obtained by Endoh and Ishikawa,[13] Fe-Mn alloys are classified into 4th

group. We compare our NMR results with these results. In the 1st type alloys of Mn-Ni and Mn-Ir, the internal field of Mn^{55} increases with the impurity concentration. This may be due to the decrease of the positive compensation in the internal field with the increase of the Ni or Ir concentration which was already discussed for dilute alloys, although the magnitude of the moment of Mn is constant. In the 2nd type alloys of Mn-Pd, the internal field of Mn^{55} increases more than that in the 1st type alloys. This is interpreted as the increase of the moment of Mn together with the decrease of positive contribution. In the 3rd type of Mn-Cu and Mn-Au alloys, the internal field of Mn^{55} slightly increases although the moment of Mn decreases. The Cu impurity seems to break the positive compensation in the γ Mn alloys more quickly than Ni or Ir impurity. The broad line width indicates the fluctuation of magnetic moments and of the degree of s-d admixture in Cu-Mn alloys. The internal field of Mn^{54} in very dilute Mn concentration alloys is -277 kOe according to the nuclear orientation experiments obtained by Campbell et al.[25] However the internal field of Mn^{55} in Cu-Mn alloys does not increase with decreasing Mn concentration as seen in figure 10. Thus, it seems that the internal field jumps discontinuously from about 55 kOe to 277 kOe. The Mn atoms that have no Mn atoms in their neighbors seem to have large magnetic moment discontinuously.

As seen in figure 13, T_2 rapidly decreases with Mn concentration, and this is an opposite tendency to usual T_2 dependence. It indicates that the electronic states in the Cu-Mn alloys drastically vary with the composition. Perhaps this is considered to be related with the drastic change of the s-d mixing in these alloys. The signals of Cu in Cu-Mn alloys are distributed in the

range below 10 kOe as seen in figure 10. It is concluded that almost all the signals are within the observation from the intensity comparison with the signals of Cu in Cu-Zn alloys. This indicates that the local field around the magnetic moments of Mn is not so large and distributed below about 10 kOe in the Cu-Mn alloys.

In the 4th type alloys of Mn-Fe, the internal field of Mn^{55} is almost constant up to the 65 at.% Fe concentration. The line width is not so broad as those in other alloys. Endoh and Ishikawa measured the average moment and the internal field of Fe.[13] According to their results, the change of the average moment is very complicated, while that of the internal field of Fe is simple. Their results are shown in Fig. 17 together with our results of the internal field of Mn. They predicted complicated change of the Mn moment from their results. From our results, however, the change of Mn seems to be simple. The situation seems not so simple and the problem remains to be solved.

Acknowledgments

The author would like to express his sincere thanks to Professors J.Itoh and K.Asayama for their continuous guidances and encouragements. He is also grateful to Dr. H.Yamagata.

References

1) S. Komura, Y. Hamaguchi, and N. Kunitomi : J.Phys.Soc.Japan 23 (1967) 171.

2) Y. Hamaguchi and N. Kunitomi : J.Phys.Soc.Japan 19 (1964) 1849.

3) A. Shibatani, K. Motizuki, and T. Nagamiya : Phys.Rev. 177 (1969) 984.

4) W. Pepperhoff and H-H. Ettwig : Z.angew.Phys. 24 (1968) 88.

5) Y. Nakai : J.Phys.Soc.Japan : 33 (1972) 1348.

6) K. Kume and T. Fujita : J.Phys.Soc.Japan 19 (1964) 1245.
Y. Masuda and K. Okamura : J.Phys.Soc.Japan 19 (1964) 1249.

7) J. Butterworth : Proc.Phys.Soc. 83 (1964) 71.

8) E. von Meerwall and D.S. Schreiber : Solid State Commun. 9 (1971) 1165.

9) D. Meneghetti and S.S. Sidhu : Phys.Rev. 105 (1957) 130.

10) G.E. Bacon, I.W. Dunmur, J.H. Smith, and R. Street : Proc.Roy.Soc. A241 (1957) 223.

11) T.J. Hicks, A.R. Pepper, and J.H. Smith : J.Phys. C1 (1968) 1683.

12) T. Yamaoka, M. Mekata, and H. Takaki : J.Phys.Soc.Japan 31 (1971) 301.

13) Y. Endoh and Y. Ishikawa : J.Phys.Soc.Japan 30 (1971) 1614.

14) S. Asano and Y. Yamashita : J.Phys.Soc.Japan 31 (1971) 1000.

15) H. Yamagata and K. Asayama : J.Phys.Soc.Japan 33 (1972) 400.

16) W.B. Mims, G.E. Devlin, S. Geschwind, and V. Jaccarino : Phys.Letters 24A (1967) 481.

17) J.C. Ho and N.E. Phillips : Phys.Letters 10 (1964) 34.

18) R.E. Watson and A.J. Freeman : Phys.Rev. 123 (1961) 2027.

19) N. Kunitomi and M. Kanashiro :. Private communication.

20) J. Korringa : Physica 16 (1950) 601.

21) Y. Obata : J.Phys.Soc.Japan 18 (1963) 1020.

22) Y. Yafet and V. Jaccarino : Phys.Rev. 133 (1964) A1630.

23) C.H. Cheng, C.T. Wei, and P.A. Beck : Phys.Rev. 120 (1960) 426.
C.H. Cheng, K.P. Gupta, E.C. van Reuth, and P.A. Beck : Phys.Rev. 126 (1962) 2030.

24) T. Moriya : J.Phys.Soc.Japan 19 (1964) 681.
R.E. Walstedt, V. Jaccarino, and N. Kaplan : J.Phys.Soc.Japan 21 (1966) 1843.

25) I.A. Campbell, J.P. Compton, I.R. Williams, and G.V.H. Wilson : Phys.Rev. Letters 19 (1967) 1319.

Figure captions

Figure 1 : Magnetic structures of a) b.c.c. Cr-Mn alloys and b) γ Mn alloys.

Figure 2 : A block diagram of pulsed NMR apparatus.

Figure 3 : The line shape of Mn^{55} in the Cr-Mn alloy of 28.9 at.% Mn.

Figure 4 : Internal field of Mn^{55} in Cr-Mn alloys is plotted versus the concentration of Mn.

Figure 5 : Full half-value width of the line shape of Mn^{55} in Cr-Mn alloys.

Figure 6 : $(T_1T)^{-1}$ of Mn^{55} in Cr-Mn alloys.

Figure 7 : The line shapes of Mn^{55} in the γ Mn alloys containing 2.5 and 5.0 at.% impurities.

Figure 8 : The line shapes of Mn^{55} in the γ Mn alloys : 10, 23, 39 at.% Ni; 10, 20, at.% Ir; 10, 18 at.% Pd; 20 at.% Au.

Figure 9 : The line shapes of Mn^{55} in the γ Mn-Fe alloys : 7.5, 15, 30, 40, 50, 65 at.% Fe. 5 at.% Cu is added to stabilize the γ phase below 40 at.% Fe.

Figure 10 : The line shapes of Mn^{55} and Cu in Mn-Cu alloys : 10, 20, 30, 40, 60, 80, 90, 95 at.% Cu. The signals above 40 MHz arise from Mn and below 10 MHz from Cu. The signals of Cu^{63} and Cu^{65} overlap because their γ values are close to each other.

Figure 11 : The center of gravity of the broad line of Mn^{55} in the figure 7, 8, 9, and 10 is plotted versus impurity concentrations.

Figure 12 : Integrated intensity of Mn^{55} signals in γ Mn alloys is plotted versus Mn concentrations. The broken line indicates the expected intensity.

Figure 13 : T_2 of Mn^{55} in Mn-Cu alloys is plotted versus Mn concentration.

Figure 14 : Internal field of Mn^{55} and W^{182} in the Cr-Mn alloys. Average magnetic moment in these alloys is also shown. H_{hf} of Mn^{55} is obtained in the present work. H_{hf} of W^{182} is adopted from ref. 19, and the moments are adopted from ref. 2.

Figure 15 : $(T_1T)^{-1/2}$ and γ versus electron concentration for paramagnetic Ti-V, V-Cr, and antiferromagnetic Cr-Mn alloys. The left hand side axis indicates the $(T_1T)^{-1/2}$ and the right, γ. The broken line in the paramagnetic region (Ti to Cr) is the translated $(T_1T)^{-1/2}$ of Mn^{55} from V^{51} multiplying by the factor 2.2 .

Figure 16 : Average magnetic moments of various γ Mn alloys are plotted versus impurity concentrations. These values are adopted from ref. 10, 11, 12, and 13. These are classified into four types. Three types are shown with solid lines. Mn-Fe alloys belong to the 4th type rather than the 1st type as mentioned in the text despite these alloys being close to the simple dilution line.

Figure 17 : Average magnetic moments and internal fields of Fe and Mn. The average moments and internal fields of Fe are adopted from ref. 13.

Table

The intensity ratio of the satellite line and the main line in the figure 7.

	IMPURITY ATOM				
CONCENT.	Ni	Pd	Cu	Au	CALCULATED
2.5 at.%	0.29	0.29	0.29	0.30	0.308
5.0 at.%	0.61	0.60	0.59	0.56	0.632

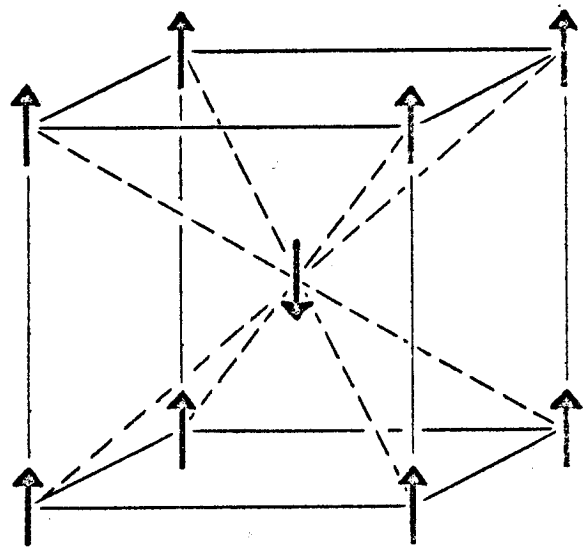

a) Cr-Mn

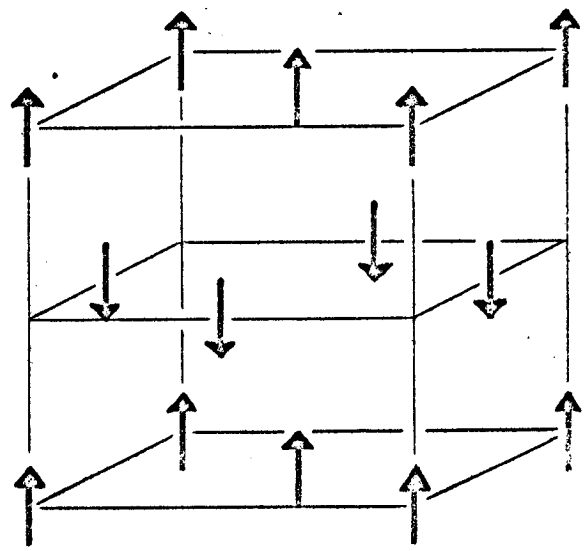

b) γ Mn

Fig. 1

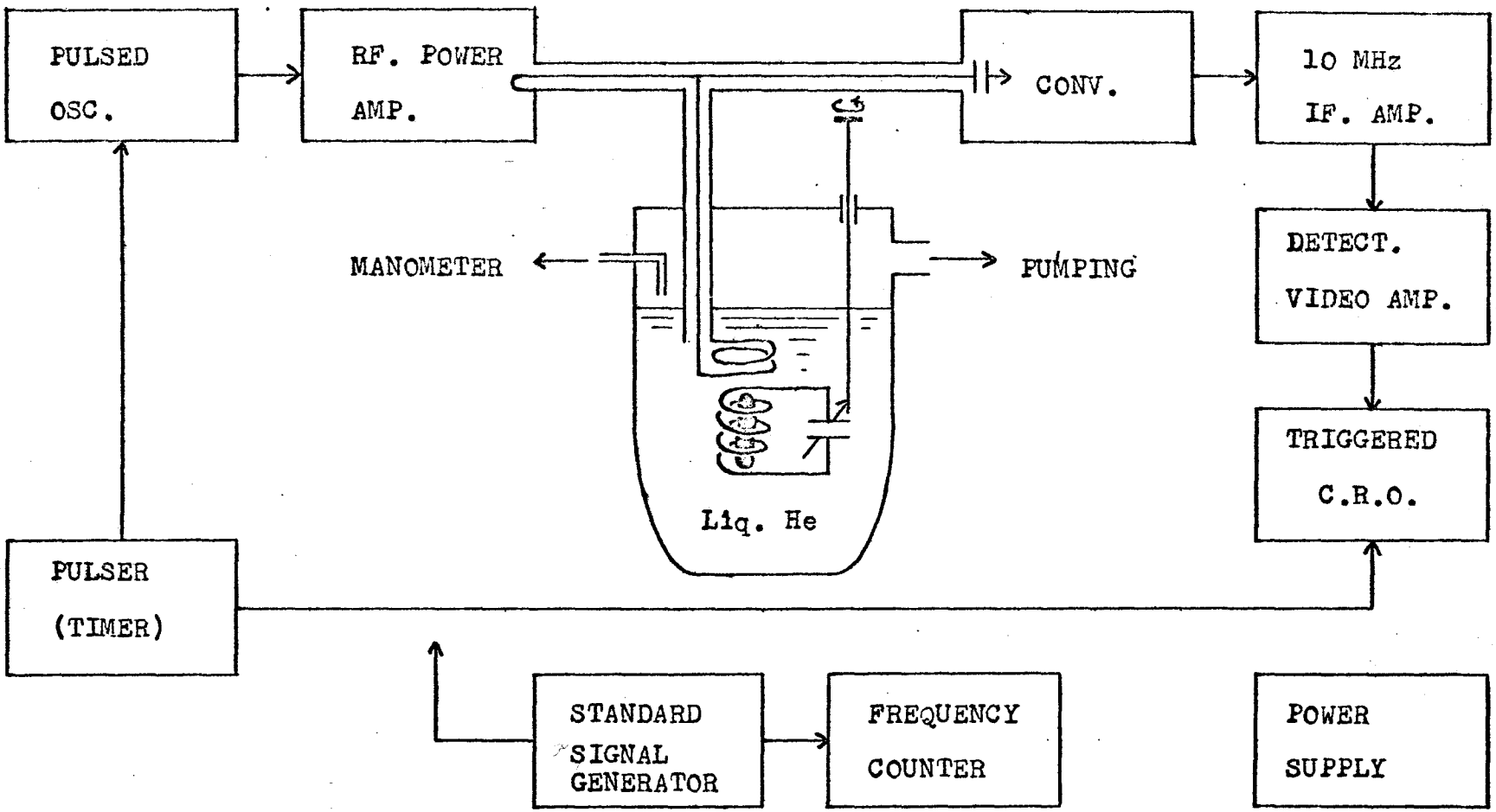
PULSED
OSC.
RF. POWER
AMP.
CONV.
10 MHz
IF. AMP.
DETECT.
VIDEO AMP.
TRIGGERED
C.R.O.
MANOMETER
PUMPING
Liq. He
PULSER
(TIMER)
STANDARD
SIGNAL
GENERATOR
FREQUENCY
COUNTER
POWER
SUPPLY

Fig.2

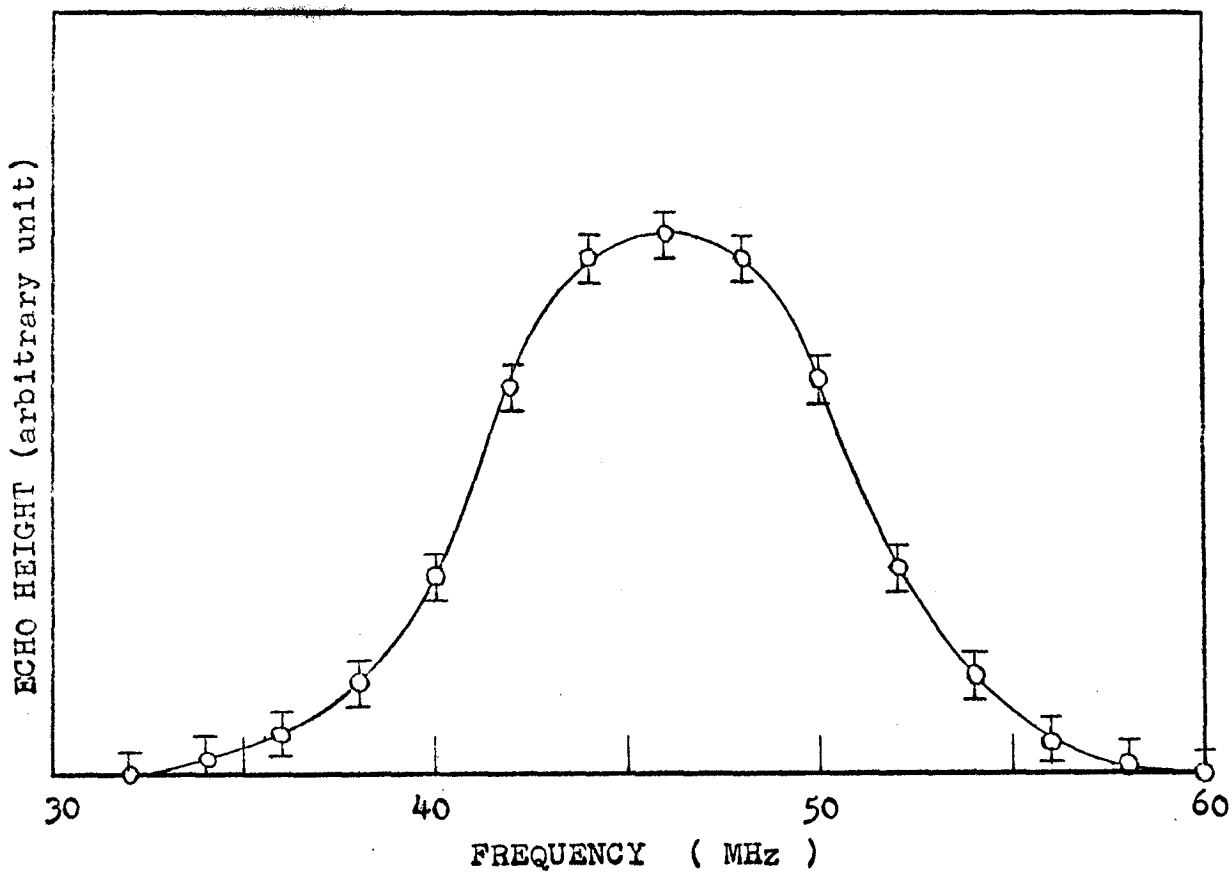

Fig. 3

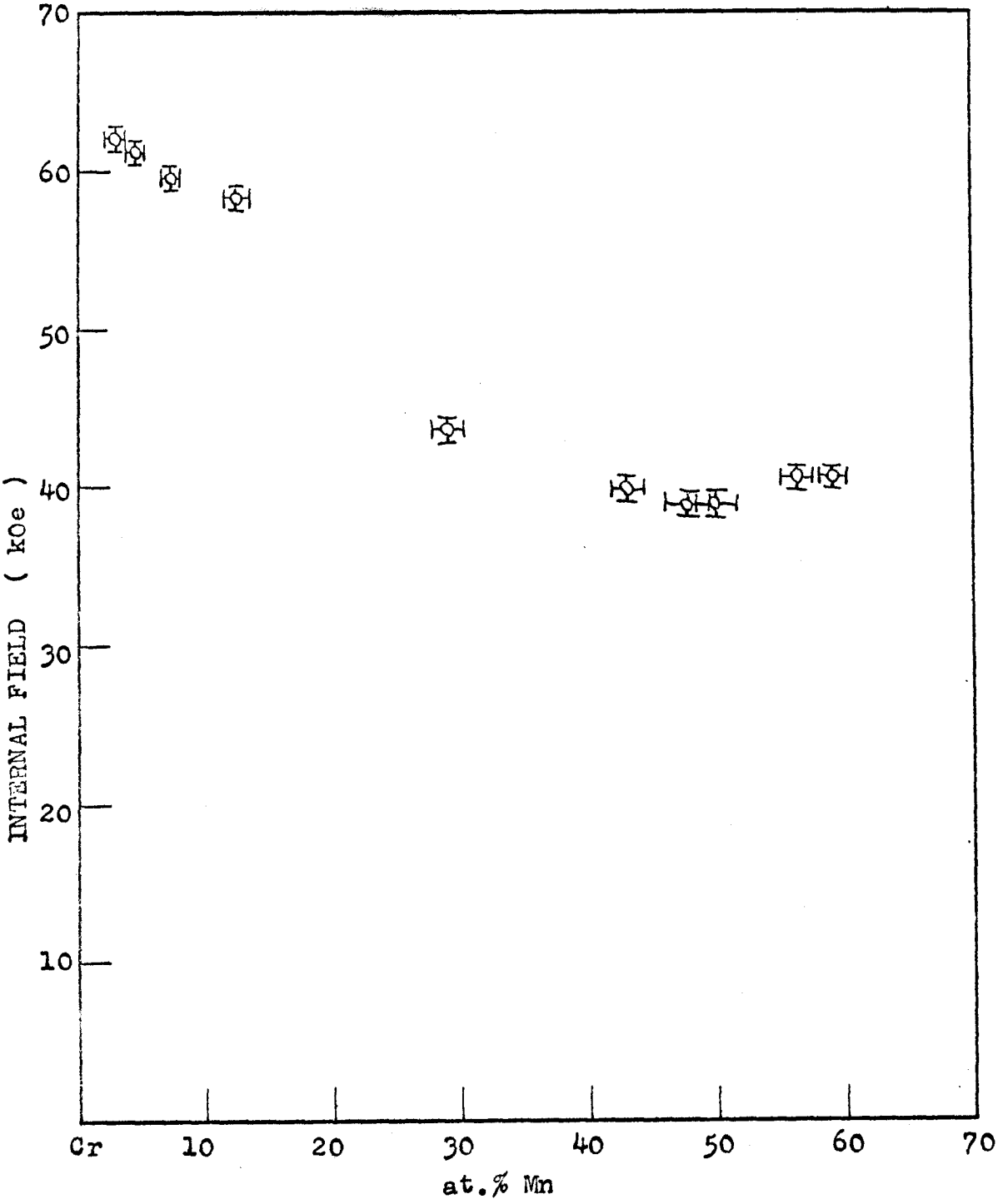
70
60
50
40
30
20
10
INTERNAL FIELD (kOe)
Cr
10
20
30
40
50
60
70
at.% Mn

Fig. 4

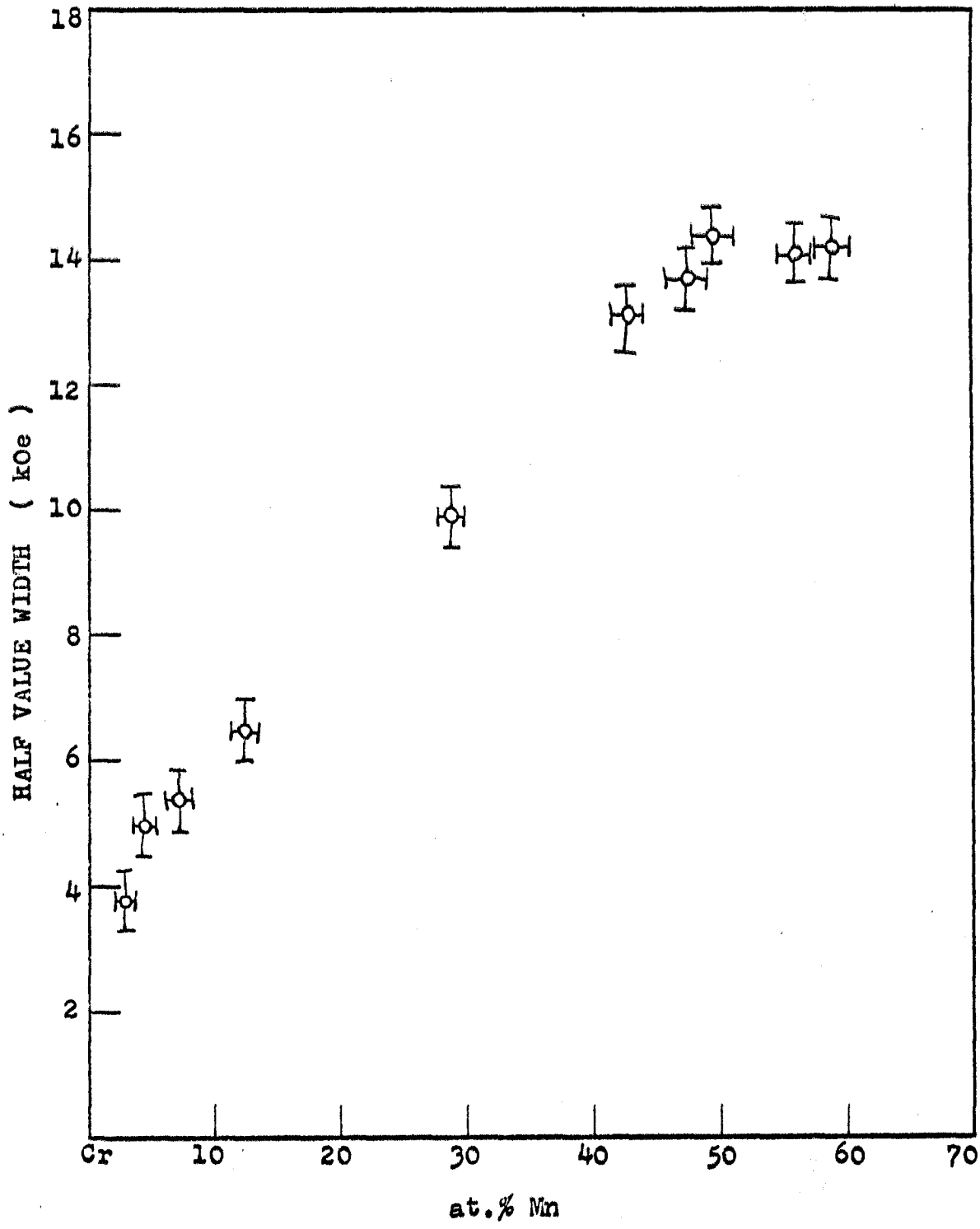
HALF VALUE WIDTH (kOe)
18
16
14
12
10
8
6
4
2
Cr
10
20
30
40
50
60
70
at.% Mn

Fig. 5

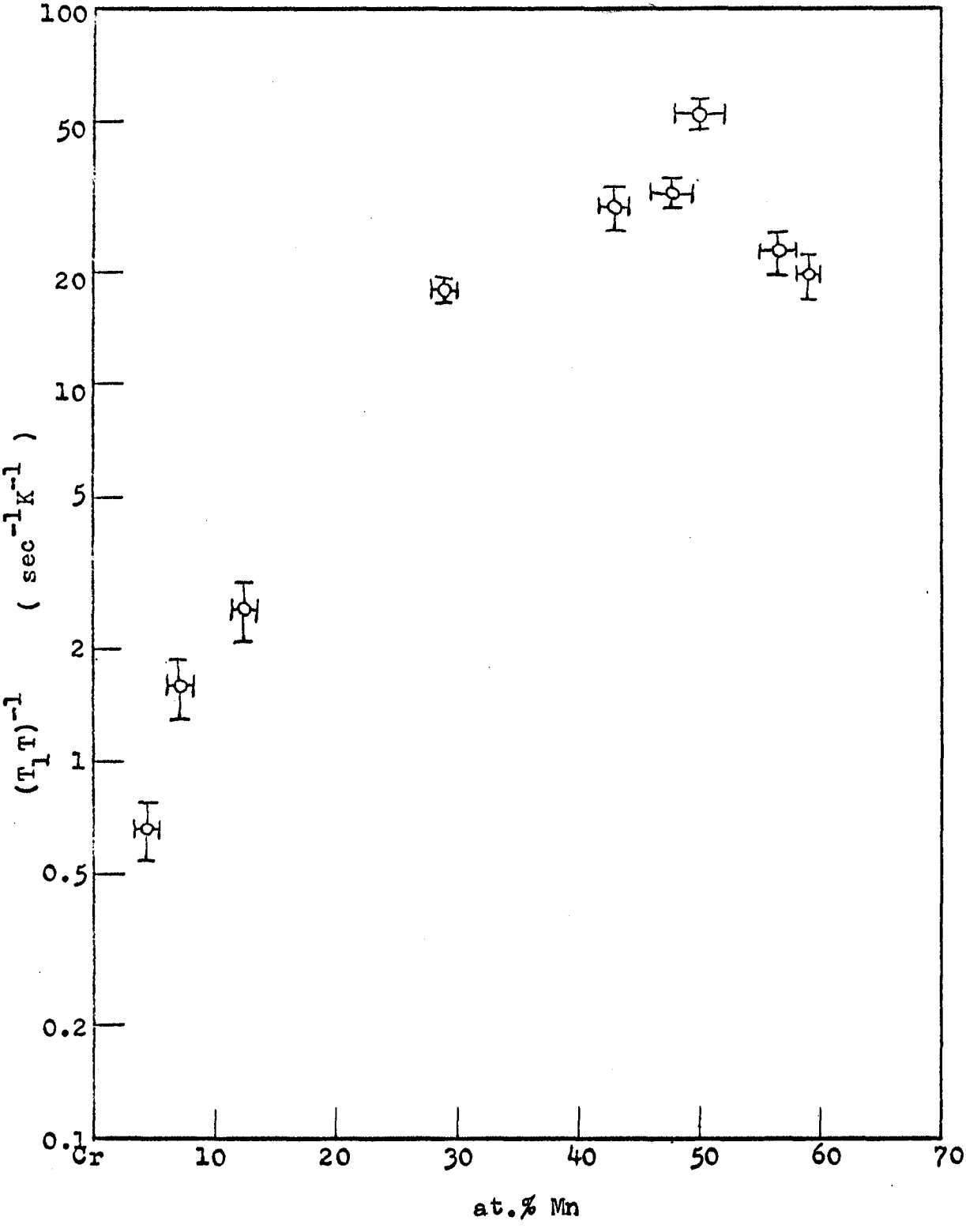

Fig. 6

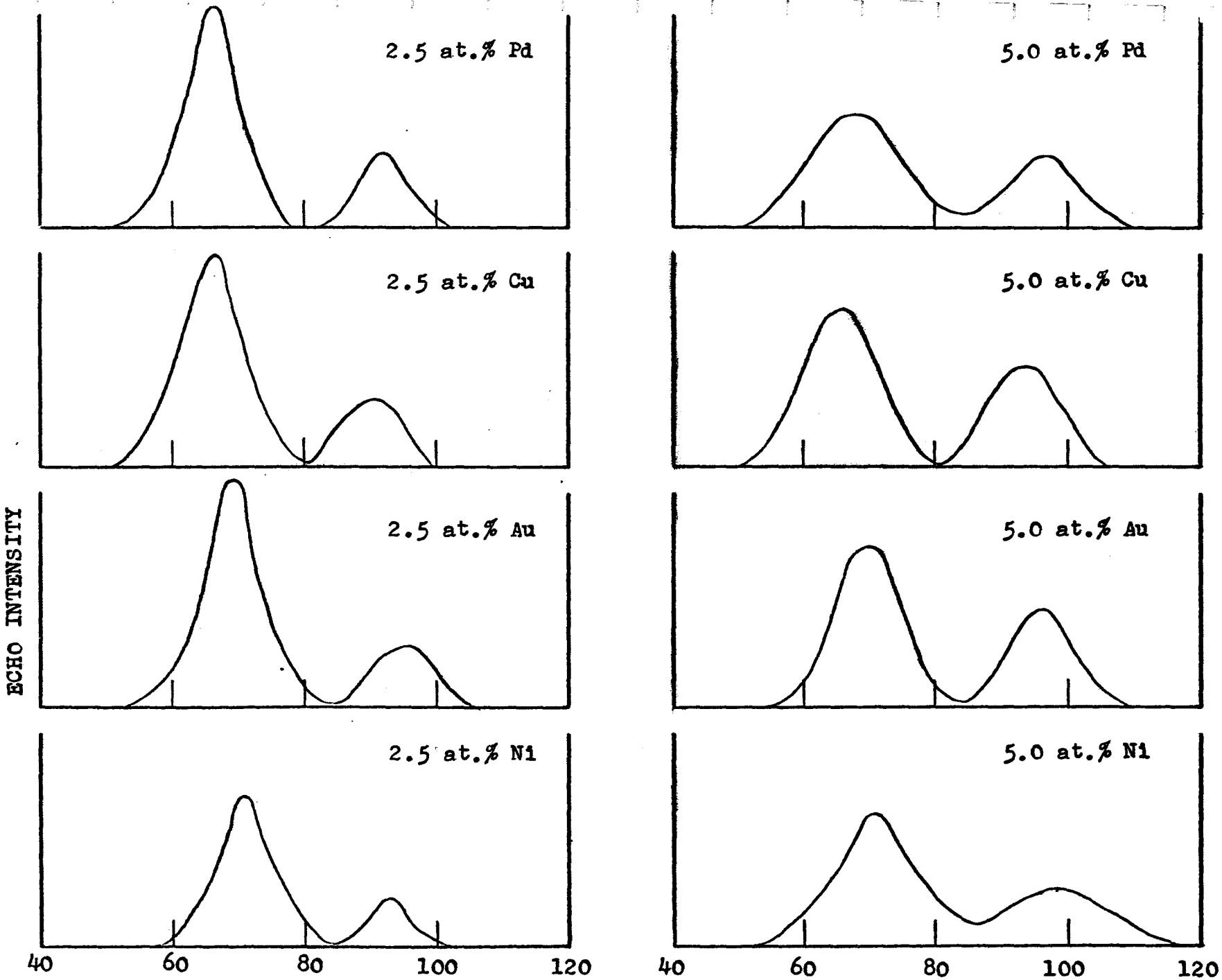
2.5 at.% Pd
5.0 at.% Pd
2.5 at.% Cu
5.0 at.% Cu
2.5 at.% Au
5.0 at.% Au
2.5 at.% Ni
5.0 at.% Ni
ECHO INTENSITY
40
60
80
100
120
INTERNAL FIELD (MHz)

Fig. 7

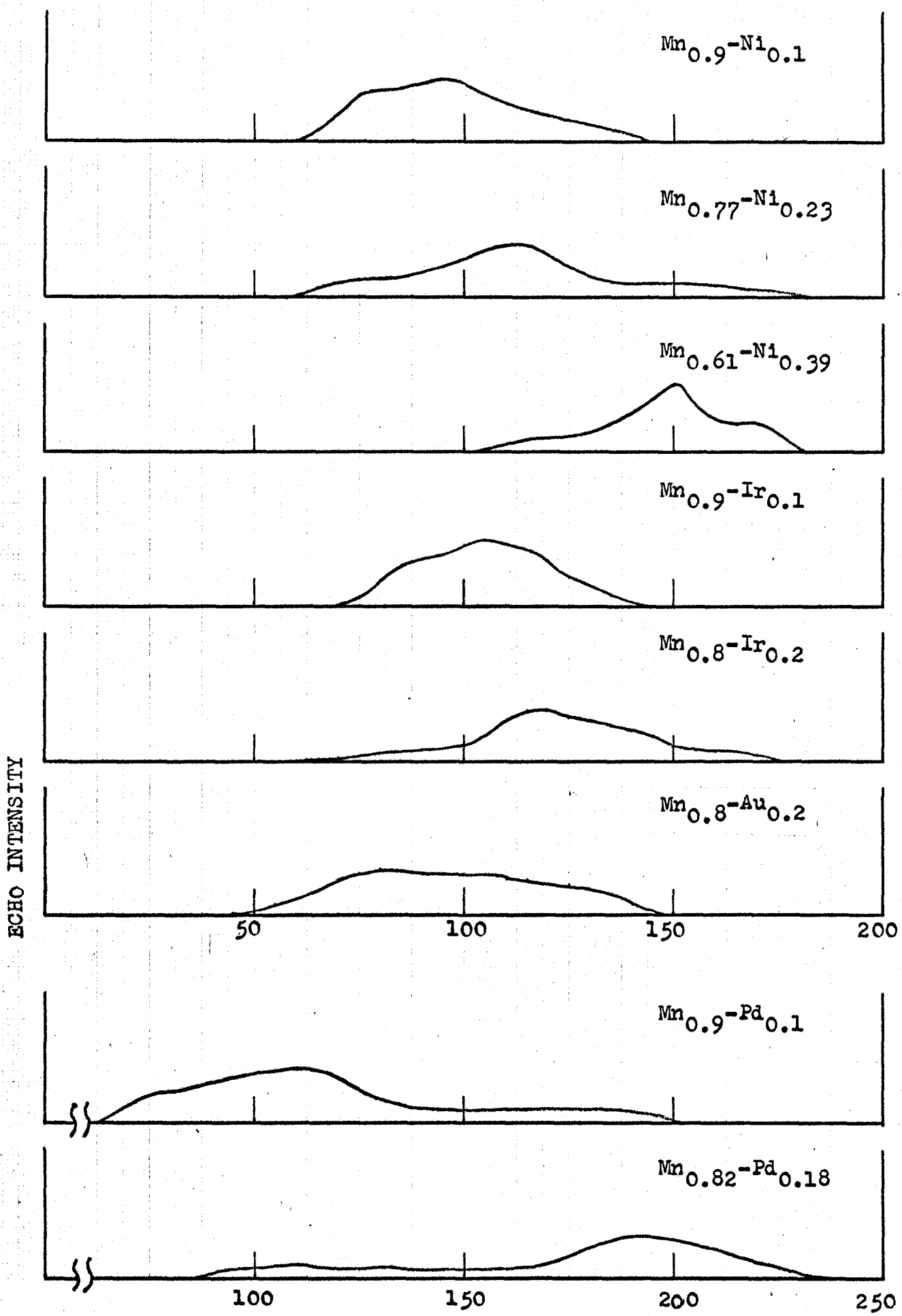
$Mn_{0.9}$-$Ni_{0.1}$
$Mn_{0.77}$-$Ni_{0.23}$
$Mn_{0.61}$-$Ni_{0.39}$
$Mn_{0.9}$-$Ir_{0.1}$
$Mn_{0.8}$-$Ir_{0.2}$
$Mn_{0.8}$-$Au_{0.2}$
$Mn_{0.9}$-$Pd_{0.1}$
$Mn_{0.82}$-$Pd_{0.18}$
ECHO INTENSITY
50
100
150
200
100
150
200
250
INTERNAL FIELD (MHz)

Fig. 8

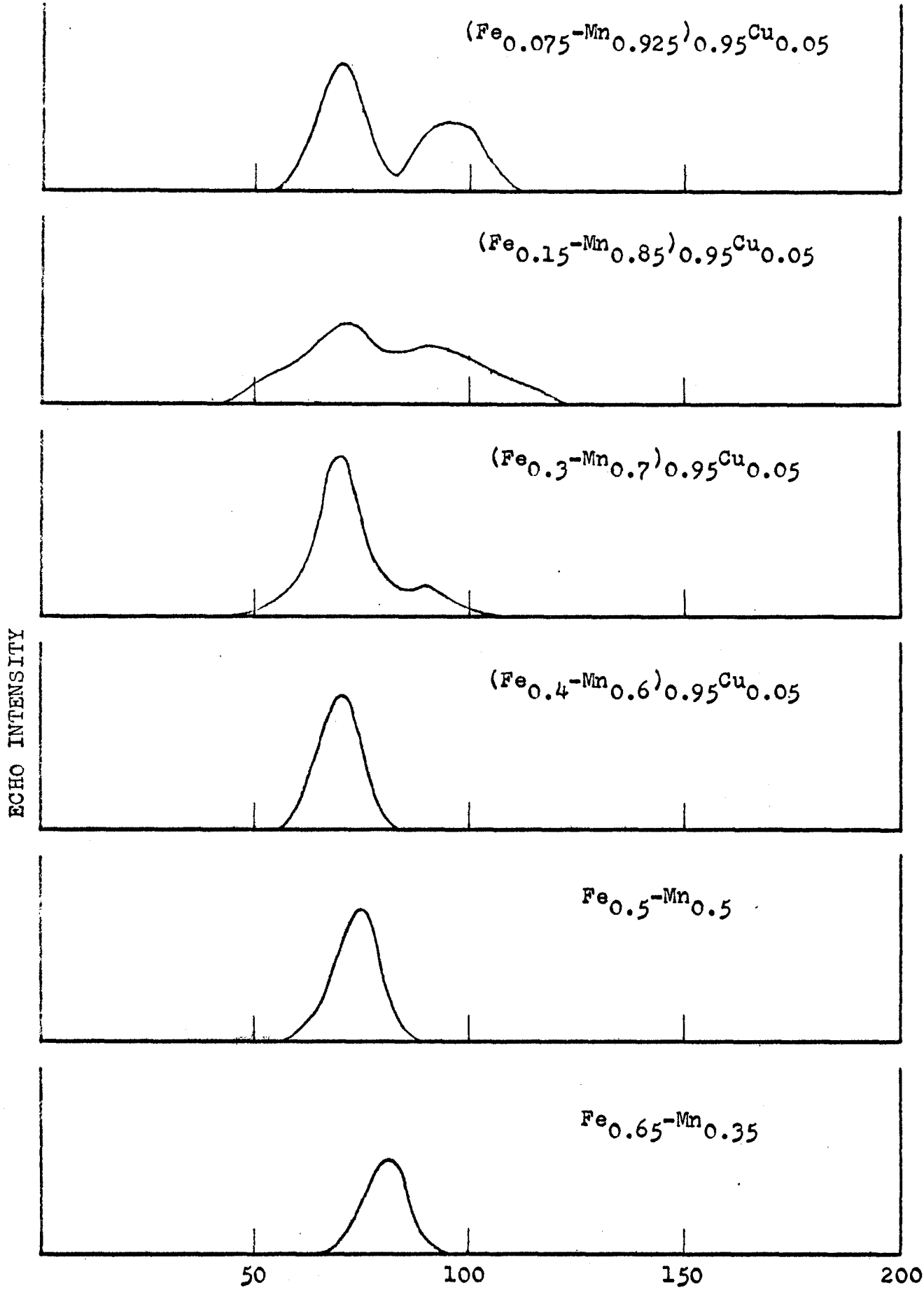
$(Fe_{0.075}-Mn_{0.925})_{0.95}Cu_{0.05}$
$(Fe_{0.15}-Mn_{0.85})_{0.95}Cu_{0.05}$
$(Fe_{0.3}-Mn_{0.7})_{0.95}Cu_{0.05}$
$(Fe_{0.4}-Mn_{0.6})_{0.95}Cu_{0.05}$
$Fe_{0.5}-Mn_{0.5}$
$Fe_{0.65}-Mn_{0.35}$
ECHO INTENSITY
50
100
150
200
INTERNAL FIELD (MHz)

Fig. 9

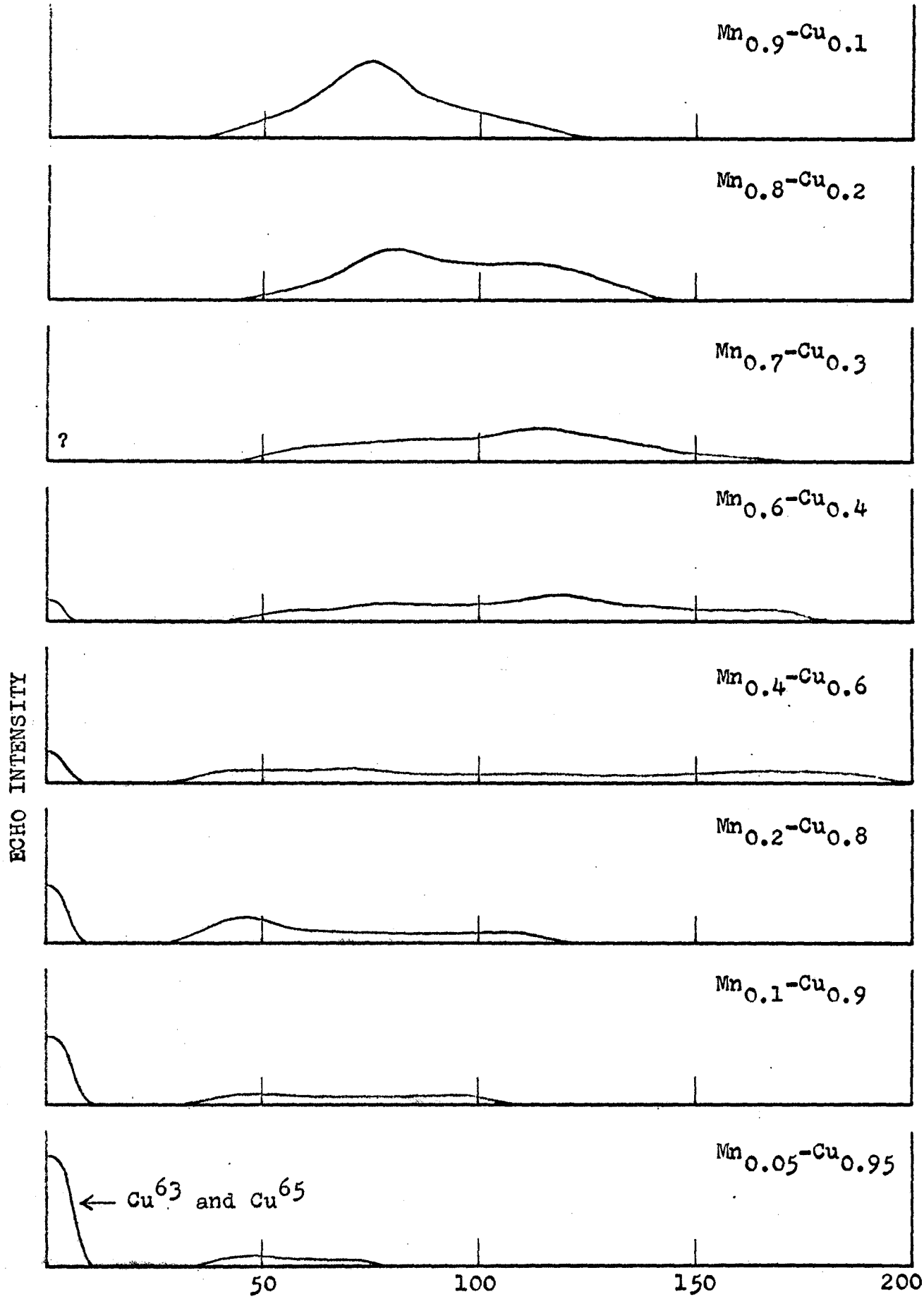
$Mn_{0.9}$-$Cu_{0.1}$
$Mn_{0.8}$-$Cu_{0.2}$
$Mn_{0.7}$-$Cu_{0.3}$
?
$Mn_{0.6}$-$Cu_{0.4}$
$Mn_{0.4}$-$Cu_{0.6}$
$Mn_{0.2}$-$Cu_{0.8}$
$Mn_{0.1}$-$Cu_{0.9}$
$Mn_{0.05}$-$Cu_{0.95}$
← Cu^{63} and Cu^{65}
ECHO INTENSITY
50
100
150
200
INTERNAL FIELD (MHz)

Fig. 10

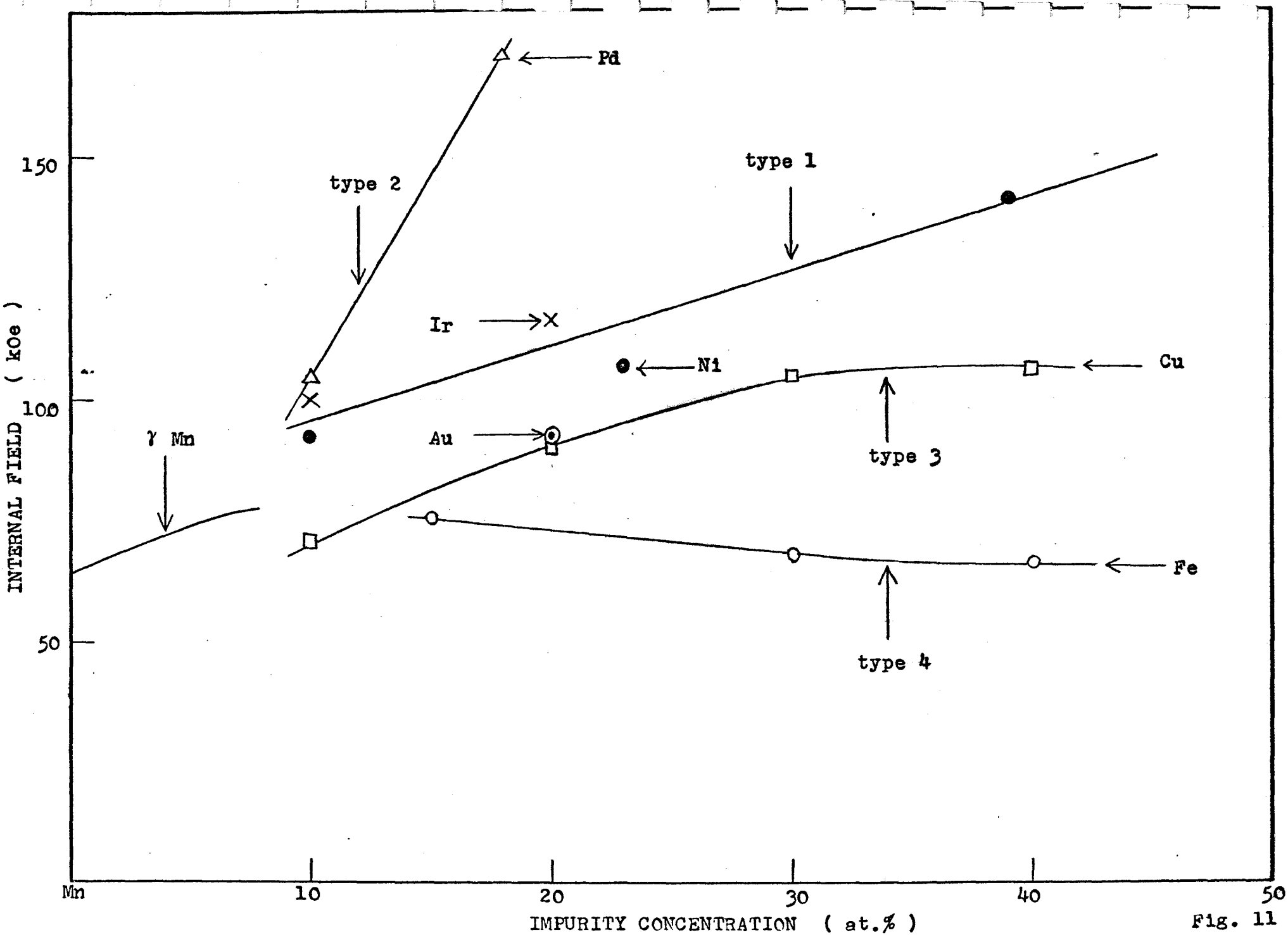
Pd
type 2
type 1
Ir
Ni
Cu
γ Mn
Au
type 3
Fe
type 4
150
100
50
INTERNAL FIELD (kOe)
Mn
10
20
30
40
50
IMPURITY CONCENTRATION (at.%)

Fig. 11

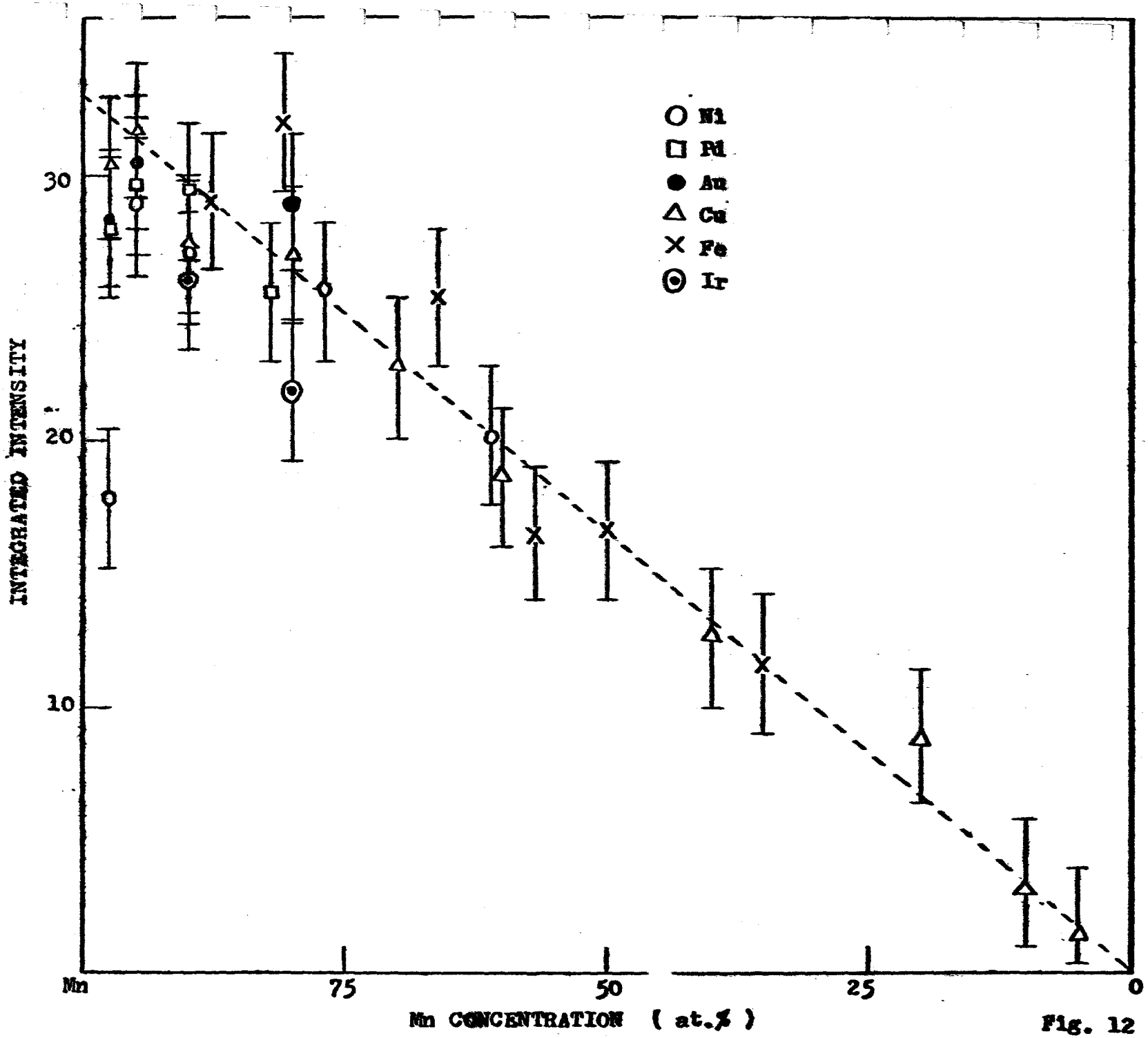
Ni
Pd
Au
Cu
Fe
Ir
INTEGRATED INTENSITY
30
20
10
Mn
75
50
25
0
Mn CONCENTRATION (at.%)

Fig. 12

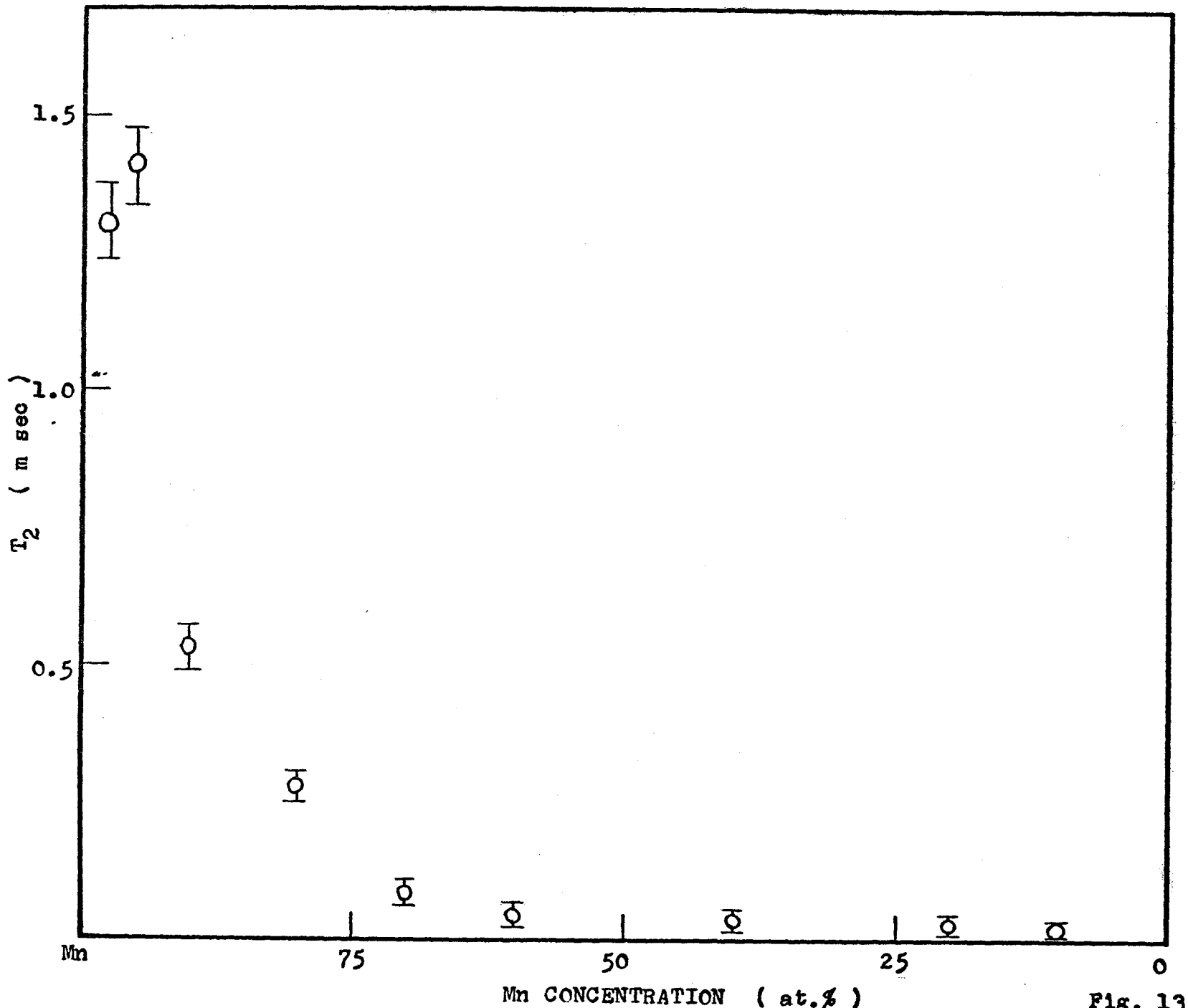

Fig. 13

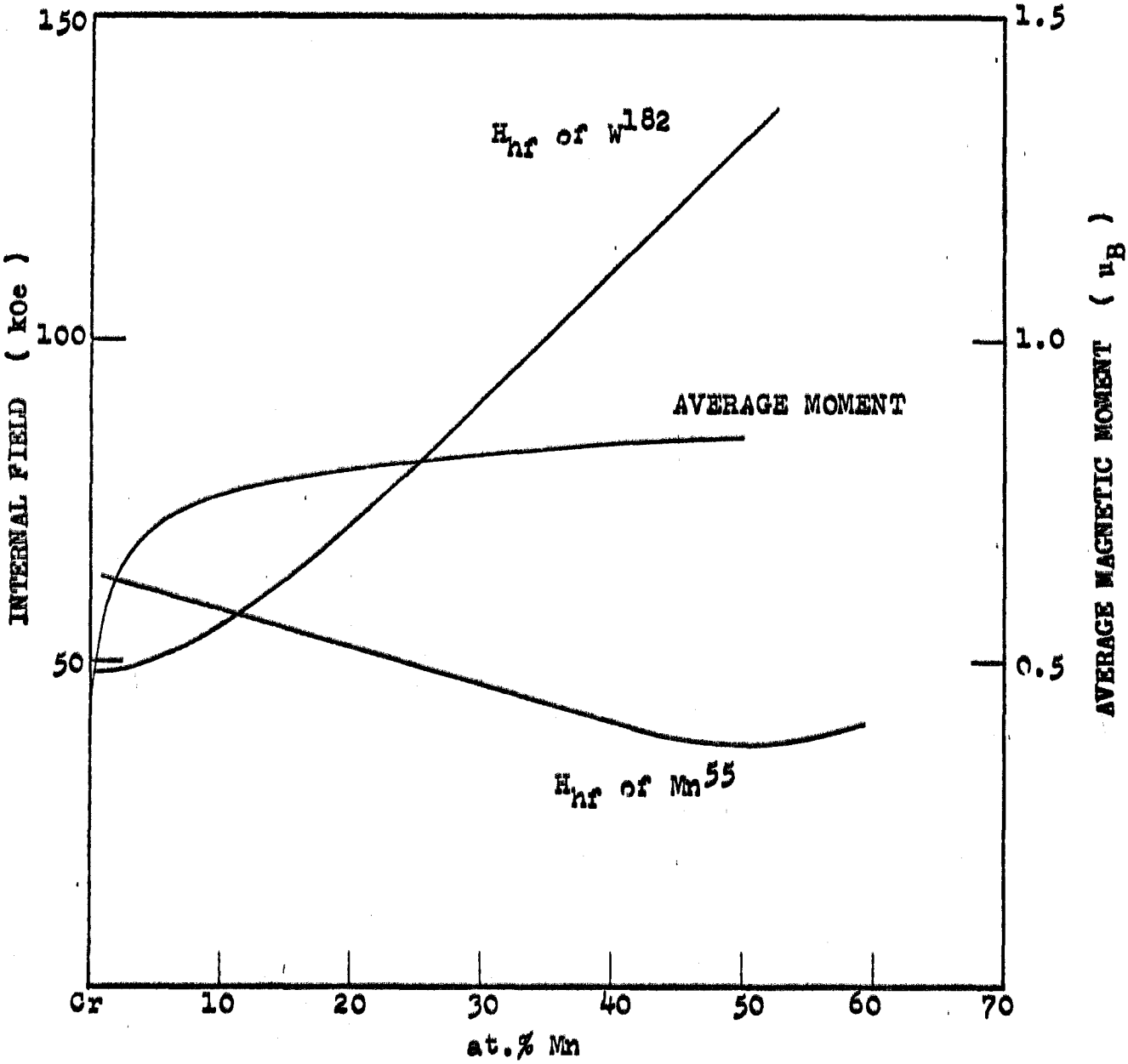
150
100
50
1.5
1.0
0.5
INTERNAL FIELD (kOe)
AVERAGE MAGNETIC MOMENT (μ_B)
H_{hf} of W^{182}
AVERAGE MOMENT
H_{hf} of Mn^{55}
Cr
10
20
30
40
50
60
70
at.% Mn

Fig. 14

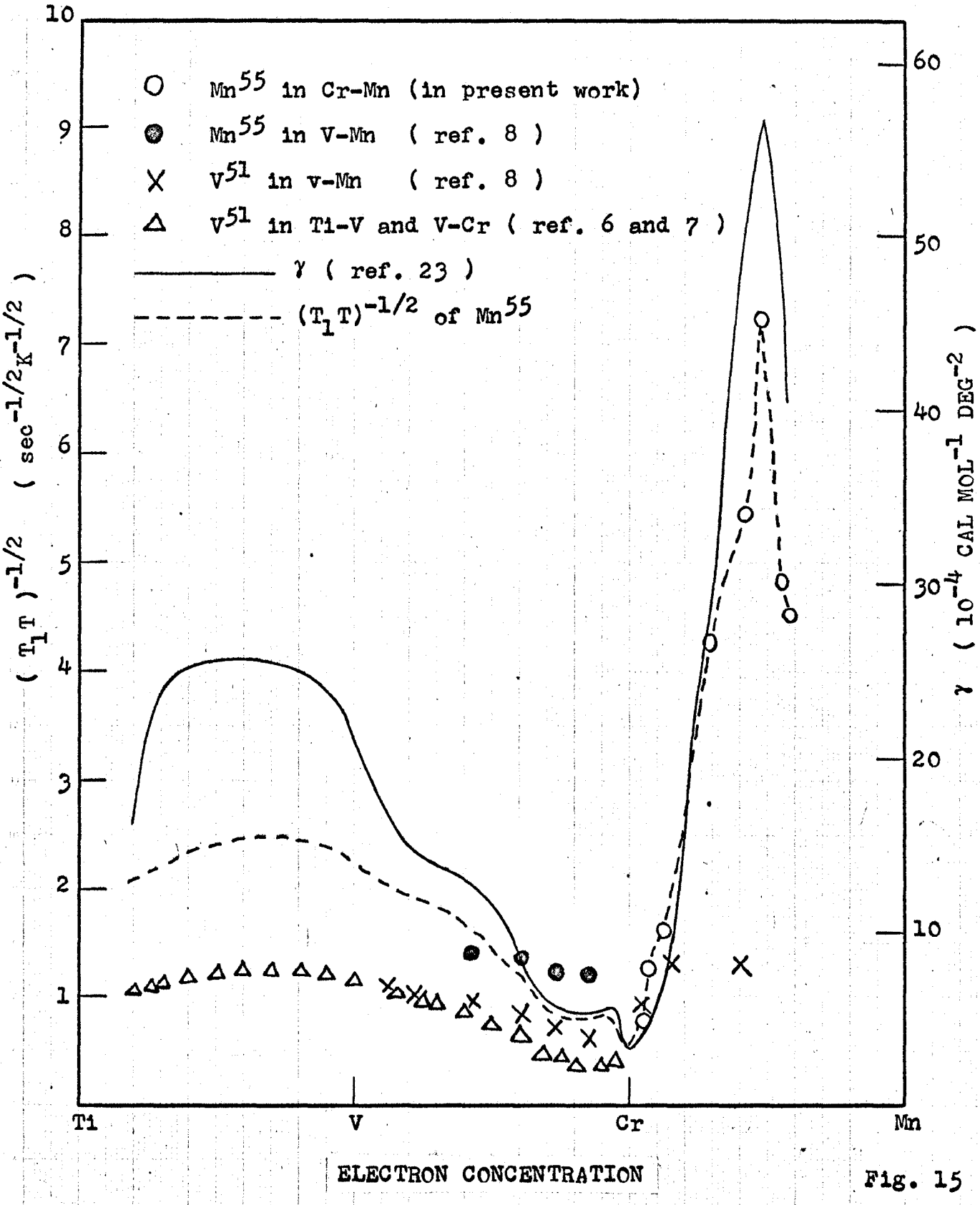
Mn55 in Cr-Mn (in present work)
Mn55 in V-Mn (ref. 8)
V51 in v-Mn (ref. 8)
V51 in Ti-V and V-Cr (ref. 6 and 7)
γ (ref. 23)
(T1T)-1/2 of Mn55
(T1T)-1/2 (sec-1/2K-1/2)
γ (10-4 CAL MOL-1 DEG-2)
10
9
8
7
6
5
4
3
2
1
60
50
40
30
20
10
Ti
V
Cr
Mn
ELECTRON CONCENTRATION

Fig. 15

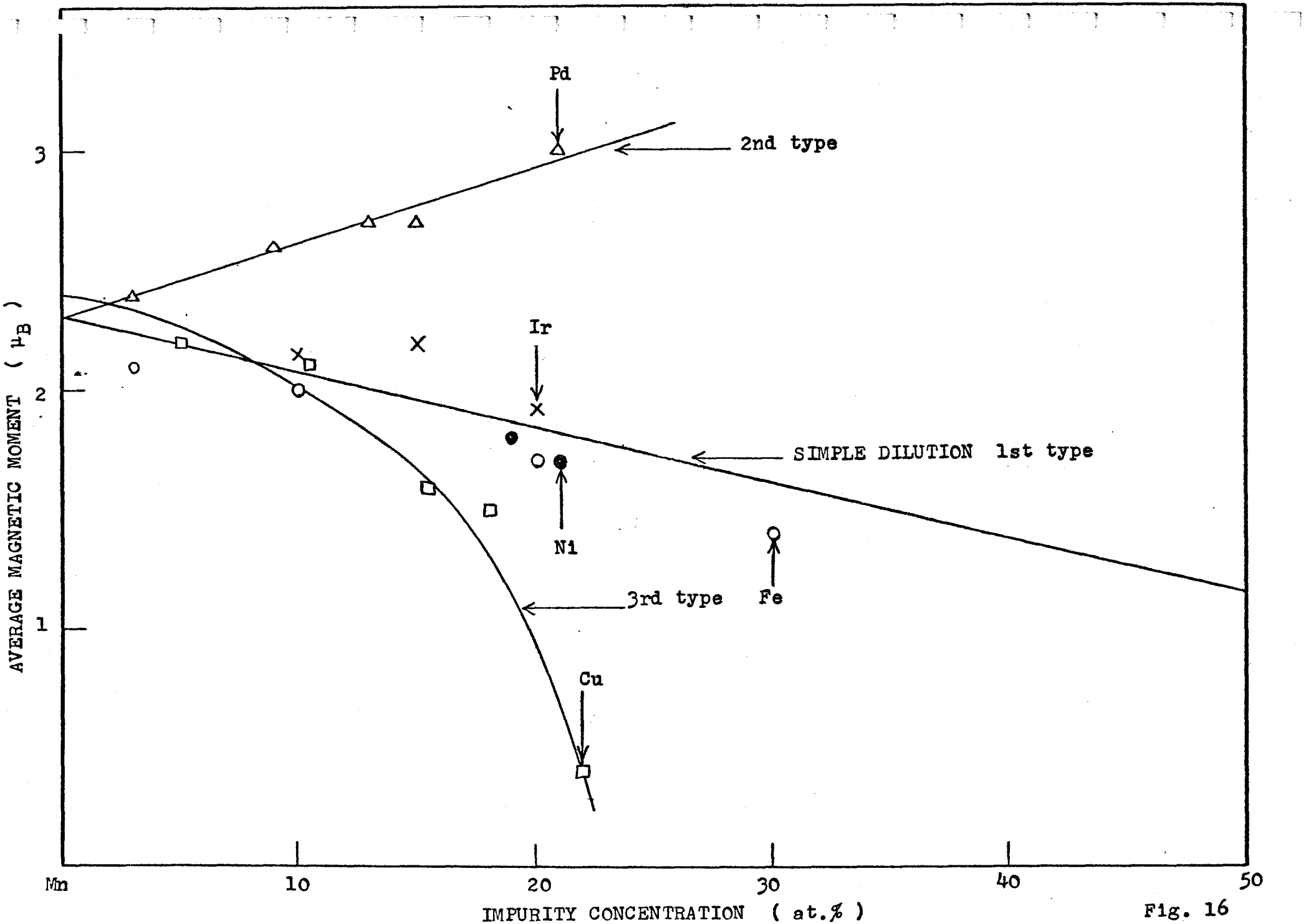
Pd
2nd type
Ir
SIMPLE DILUTION 1st type
Ni
Fe
3rd type
Cu
AVERAGE MAGNETIC MOMENT (μ_B)
3
2
1
Mn
10
20
30
40
50
IMPURITY CONCENTRATION (at.%)

Fig. 16

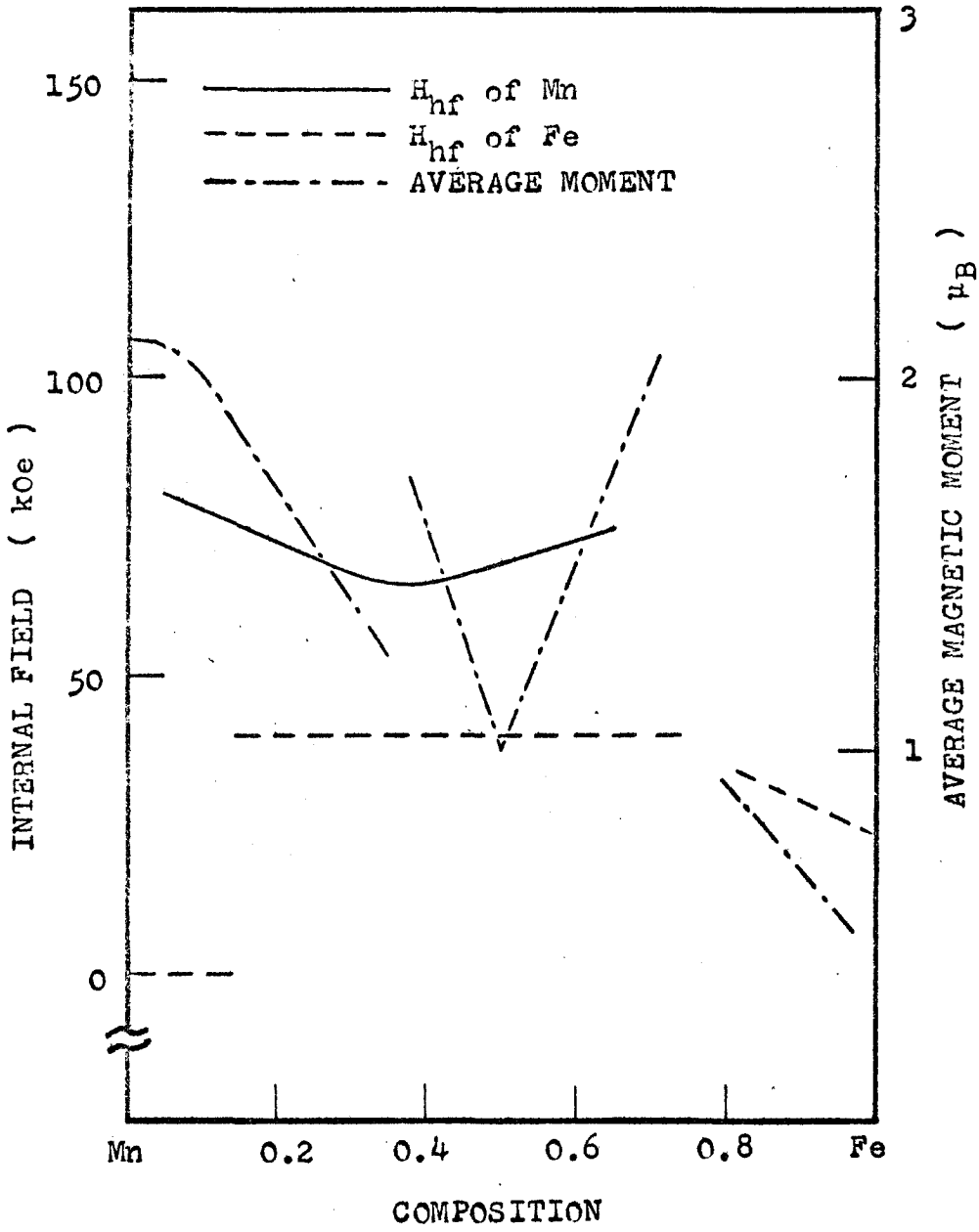
150
100
50
0
3
2
1
H_{hf} of Mn
H_{hf} of Fe
AVERAGE MOMENT
INTERNAL FIELD (kOe)
AVERAGE MAGNETIC MOMENT (μ_B)
Mn
0.2
0.4
0.6
0.8
Fe
COMPOSITION

Fig. 17